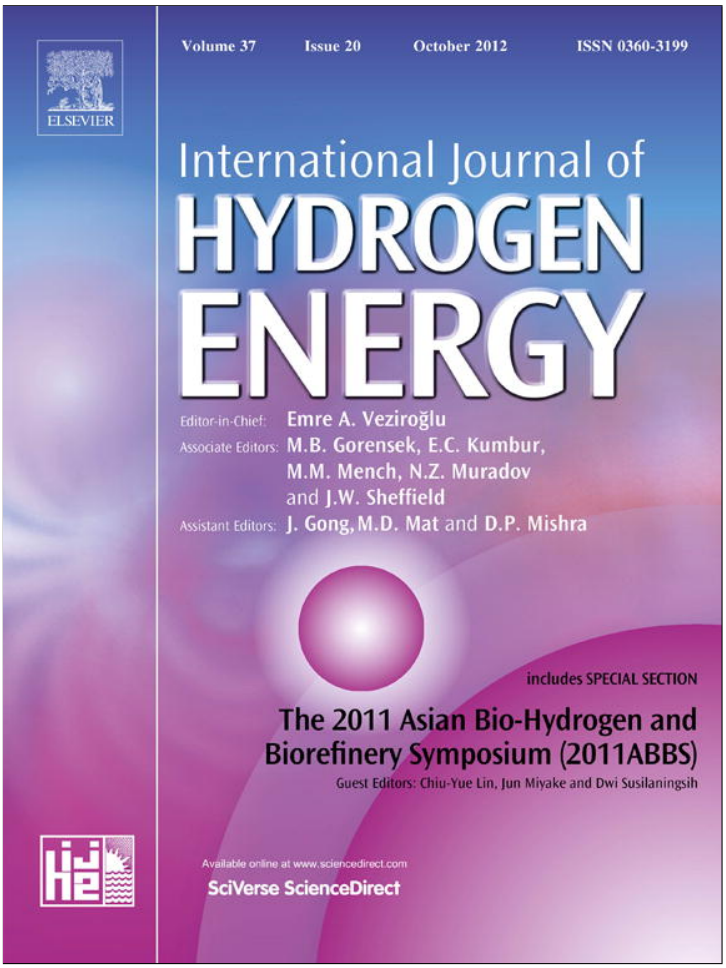

INTERNATIONAL JOURNAL OF HYDROGEN ENERGY 37 (2012) 15766–15777

Available online at www.sciencedirect.com

SciVerse ScienceDirect

journal homepage: www.elsevier.com/locate/he

Parameter sensitivity examination for a complete three-dimensional, two-phase, non-isothermal model of polymer electrolyte membrane fuel cell

Xiao-Dong Wang [a,b,*], *Jin-Liang Xu* [a,b], *Duu-Jong Lee* [c,d]

[a] *State Key Laboratory of Alternate Electrical Power System with Renewable Energy Sources, North China Electric Power University, Beijing 102206, China*

[b] *Beijing Key Laboratory of Multiphase Flow and Heat Transfer for Low Grade Energy, North China Electric Power University, Beijing 102206, China*

[c] *Department of Chemical Engineering, College of Engineering, National Taiwan University of Science and Technology, Taipei 106, Taiwan*

[d] *Department of Chemical Engineering, National Taiwan University, Taipei 106, Taiwan*

ARTICLE INFO

Article history:
Received 2 March 2012
Received in revised form
4 April 2012
Accepted 5 April 2012
Available online 4 May 2012

Keywords:
Polymer electrolyte membrane fuel cell
Two-phase
Non-isothermal
Model
Parameter sensitivity analysis
Parallel flow field

ABSTRACT

Parameter sensitivity analysis is carried out for a complete three-dimensional, two-phase, non-isothermal model of polymer electrolyte membrane (PEM) fuel cell with a parallel flow field design. The model couples the two-phase flow of the multi-component reactants and liquid water, species transport, electrochemical reactions, proton and electron transport, and the electro-osmosis transport, back diffusion of water in the membrane, and energy transport. Twenty nine parameters, which are classified into the structural or transport parameters of porous layers (tortuosity, porosity, permeability, proton conductivity, electron conductivity, and thermal conductivity) as well as the electrochemical parameters (anodic and cathodic exchange current densities, anodic and cathodic transfer coefficients for anode and cathode reactions), are used to implement individual parameter investigation. The results show the parameters can be divided in to strongly sensitive, conditional sensitive and weak sensitive parameters according to its effect on the cell polarization curve. The optimization of parameters of cathode gas diffusion layer (GDL) and catalyst layer (CL) is more important to improve cell performance than that of anode GDL and CL because liquid water transport and removal affect significantly membrane hydration and reactant transport. Electrochemical parameters determine the activation potential and the slope of ohmic polarization hence these parameters can be used to fit experimental polarization curve more effectively than the other parameters.

1. Introduction

PEM fuel cells, which are electrochemical devices that efficiently convert reactant chemical energy directly into electrical energy, are considered to be one of the most promising alternative clean power generators for portable, mobile and stationary applications because of its low to zero emissions, low-temperature operation, high power density and fast start-up [1–14].

The performance of PEM fuel cells depends strongly on the material characteristics, mechanical design (particularly the

* *Corresponding author*. State Key Laboratory of Alternate Electrical Power System with Renewable Energy Sources, North China Electric Power University, Beijing 102206, China. Tel./fax: 86 10 62321277.
E-mail address: wangxd99@gmail.com (X.-D. Wang).

0360-3199/$ – see front matter
doi:10.1016/j.ijhydene.2012.04.029

Nomenclature:

Aj_0^{ref}	exchange current density, A m^{-3}
C	mass fraction
C_F	quadratic drag factor
D	mass diffusivity, m^2 s^{-1}
D_λ	water diffusivity in the membrane
F	Faraday constant, 96,487 C/mol
i	current density, A m^{-2}
I	average current density in the fuel cell, A m^{-2}
j	transfer current density, A m^{-3}
k_c	coefficient of water vapor condensation rate, s^{-1}
k_e	coefficient of water vapor evaporation rate, atm^{-1} s^{-1}
k_{rl}	relative permeability of the liquid water
k_p	permeability, m^2
k_{rg}	relative permeability of the gaseous mixture
M	molecular weight, kg mol^{-1}
M_m	membrane equivalent weight, kg mol^{-1}
n_d	Electro-osmotic drag coefficient
p	pressure, atm
p_c	capillary pressure, atm
p_{sat}	saturated water vapor pressure, atm
R	universal gas constant, 8.314 J mol^{-1} K^{-1}
s	liquid water saturation
S_c	source term in the species equation
S_j	source term in the phase potential equation
S_L	source term accounting due to phase change of water
$S_{\vec{u}}$	source term in the momentum equation
T	cell temperature, K
$\vec{u}$	velocity vector, m s^{-1}
V_{cell}	operating voltage, V
x_{H_2O}	mole fraction of water vapor
x,y,z	x,y, and z direction coordinates, m

Greek

$\alpha_{a,a}$	anodic transfer coefficient for anode reaction
$\alpha_{a,c}$	cathodic transfer coefficient for anode reaction
$\alpha_{c,a}$	anodic transfer coefficient for cathode reaction
$\alpha_{c,c}$	cathodic transfer coefficient for cathode reaction
ε	porosity
η	overpotential, V
η_m	Ohmic overpotential in the membrane, V
θ	contact angle of water on the porous material, arc
λ	water content in membrane
μ	viscosity, kg m^{-1} s^{-1}
ρ	density, kg m^{-3}
ρ_{dry}	membrane dry density, kg m^{-3}
σ	surface tension, N m^{-1}
σ_m	proton conductivity, S m^{-1}
σ_s	electron conductivity, S m^{-1}
τ	tortuosity of the pores in the porous material
Φ_m	ionic phase potential, V
Φ_s	electronic phase potential, V

Subscripts

a	anode
c	cathode
eff	effective
g	gaseous phase
H_2	hydrogen
H_2O	water
k	kth species of the mixture
l	liquid phase
O_2	oxygen
porous	porous medium
ref	reference value
sat	saturation
total	total

flow field design in the bipolar plates) and the operating conditions [15]. The objective of the optimization of the flow field design and operating conditions is to enhance the reactant transport to the porous GDLs and CLs for participating in the electrochemical reactions, which is closely related to the water (liquid and vapor) transport in the cell. Water management is critical to the PEM fuel cell performance. It is well known that the currently used commercial polymer electrolyte membranes in PEM fuel cells must be well hydrated to maintain high proton conductivity, which is proportional to the water content in the membrane. Decreasing of the water content in the membrane leads to reduced performance due to increases of the voltage loss in the membrane. To avoid membrane dehydration, the inlet flows are usually injected with water vapor. In addition, the electrochemical reactions at the cathode produce water vapor, which may condense and accumulate in the pores of the porous layers and water is also transported from the anode to the cathode by electro-osmosis. Excessive liquid water can cause flooding of the pores in the cathode GDL and the CL, thus increasing the mass transfer resistance to the reactant flow. Therefore, understanding and control of the water transport in the cell are important for improving cell performance.

At present, the local distributions and transport of reactants in the cell are difficult to measure due to the small cell sizes; thus, numerical modeling and simulations have been extensively used in research and for industrial applications of PEM fuel cells to give to a better understanding of the physicochemical phenomena occurring in the cell and to provide a useful tool for optimizing fuel cell systems. If the model properly describes the phenomena that primarily influence the physicochemical effects as validated by experimental results, the model can provide insights into the choice of materials, geometric parameters, and operating conditions to obtain the best performance in the fuel cell system through optimization studies. Many PEM fuel cell models have been developed in the past decade, and they can generally be classified into one-, two- and three-dimensional, single-phase and two-phase, isothermal and non-isothermal, steady and transient models [16–29].

PEM fuel cells involve multiple complex transport and electrochemical phenomena including two-phase flow and diffusion of multi-component reactant gases and liquid water

in the micro-channels and porous layers, heat transfer and phase change, catalyst–electrochemical reactions on the pore surface in the porous CL, and electron and proton transport. These phenomena are coupled with each other and occur at disparate length and time scales. Because of the complexity, generally the PEM fuel cell involves a large number of empirical or experimental parameters. In the previous investigations different parameter values were adopted due to model differences, and some parameters have a wide value range in different models. The parameter sensitivity analysis is important for PEM fuel cell modeling and simulations, which can not only provide a proper parameter selection to fit experimental polarization curves but also understand parameter discrepancy between different models. Furthermore, the parameter sensitivity analysis also provides useful information to material design of fuel cells. The parameters which have significant effect on the cell performance should be optimized, but the parameters which have a little effect on the cell performance will not be taken care in the material design. Although some parameter sensitivity analyses have been conducted in the previous investigations [24,30], the models were single-phase or isothermal, even though two-phase and non-isothermal model was adopted, the water transport in the membrane did not include properly. Thus, a complete PEM fuel cell model has to be developed to implement the parameter sensitivity analysis and the model at least should be three-dimensional, two-phase, and non-isothermal due to importance of water and thermal managements in PEM fuel cells.

Based on the analysis above, this work develops a complete three-dimensional, two-phase, non-isothermal model for a PEM fuel cell based on the two-fluid approach, in which the two-phase flow of the multi-component reactants and liquid water are coupled with the species transport, electrochemical reactions, proton and electron transport, electro-osmosis and back diffusion of water. Different two liquid water transport equations were developed for the various cell units based on the different liquid water transport mechanisms in the fuel cell. The model is used to implement the parameter sensitivity analysis. Twenty nine parameters, which are classified into the structural or transport parameters of porous layers (tortuosity, porosity, permeability, proton conductivity, electron conductivity, and thermal conductivity) as well as the electrochemical parameters (anodic and cathodic exchange current densities, anodic and cathodic transfer coefficients for anode and cathode reactions), are examined.

2. Model

A three-dimensional, two-phase, non-isothermal PEM fuel cell model is developed by using two-fluid approach. The model comprises the anode flow channel, the anode GDL, the anode CL, the proton exchange membrane, the cathode CL, the cathode GDL, and the cathode flow channel. The parallel flow field design is adopted. Due to symmetry, only a periodic part is chosen as computational domain, which includes a half flow channel and a half rib as shown in Fig. 1. The geometric parameter is listed in Table 1.

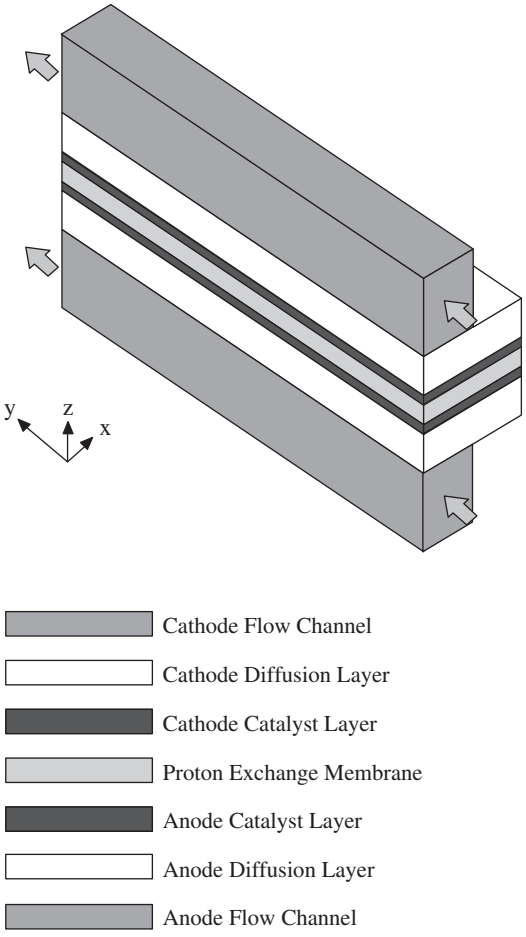

Fig. 1 – Schematic of computational domain.

The model adopts the following assumptions: 1) the fuel cell operates at steady state; 2) the gaseous species are ideal gases; 3) the reactant flow in the channel is laminar; 4) the diffusion layer, catalyst layer and membrane are isotropic porous layers; 5) water produced in the cathode catalyst layer is in the vapor phase. Table 2 lists the basic governing equations, which include the mass, momentum, and species equations for gaseous species, the liquid water transport equation in the channel, gas diffusion layer and catalyst layer, the water content equation in the membrane, the electrical potential conservation equations, and energy equation.

Table 1 – Geometric parameters of fuel cell.

Parameter	Value	Unit
Channel length	100	mm
Channel width	1	mm
Channel height	1	mm
Rib width	1	mm
Thickness of GDL	0.3	mm
Thickness of CL	0.005	mm
Thickness of membrane	0.035	mm

Table 2 – Governing equation and source term [1,15,16,19].

Governing equation	Mathematical expressions	Source term and transport properties
Gaseous continuity equation	$\nabla\cdot(\rho_g\vec{u}_g)=\begin{cases}S_{c,H_2} & \text{anode}\\ S_{c,H_2O}+S_{c,O_2}-S_L & \text{cathode}\end{cases}$	$S_{c,H_2}=-(j_a/2F)M_{H_2}$, $S_{c,O_2}=-(j_c/4F)M_{O_2}$, $S_{c,H_2O}=(j_c/2F)M_{H_2O}$, $j_a=Aj_{0,a}^{ref}\left(\frac{C_{H_2}}{C_{H_2}^{ref}}\right)^{1/2}\left[e^{(\alpha_{a,a}F/RT)\eta}-\frac{1}{e^{(\alpha_{a,c}F/RT)\eta}}\right]$, $j_c=Aj_{0,c}^{ref}\left(\frac{C_{O_2}}{C_{O_2}^{ref}}\right)\left[e^{(\alpha_{c,a}F/RT)\eta}-\frac{1}{e^{(\alpha_{c,c}F/RT)\eta}}\right]$,
Gaseous momentum equation	$\frac{1}{\varepsilon^2(1-s)^2}\nabla\cdot(\rho_g\vec{u}_g\vec{u}_g)$ $=-\nabla p_g+\frac{1}{\varepsilon(1-s)}\nabla\cdot(\mu_g\nabla\vec{u}_g)+S_{\vec{u}}$	$S_L=M_{H_2O}k_c\frac{\varepsilon(1-s)x_{H_2O}}{RT}(p_{H_2O}-p_{sat})$ if $p_{H_2O}>p_{sat}$, $S_L=k_e\varepsilon s\rho_l(p_{H_2O}-p_{sat})$ if $p_{H_2O}<p_{sat}$, $p_{sat}=10^{-2.1794+0.02953T-9.1837\times10^{-5}T^2+1.4454\times10^{-7}T^3}$ $S_{\vec{u}}=-\frac{\mu_g\vec{u}_g}{k_pk_{rg}}-\frac{\varepsilon C_F\rho_g}{\sqrt{k_p}}\lvert\vec{u}_g\rvert\vec{u}_g$
Gaseous species equation	$\nabla\cdot(\rho_g\vec{u}_gC_k)=\nabla\cdot(\rho_gD_{k,eff}\nabla C_k)+S_c-S_L$	$D_{k,eff}=D_k\varepsilon_{eff}^{\tau}$, $\varepsilon_{eff}=\varepsilon(1-s)$, $\eta=\Phi_s-\Phi_m$ on the anode side, $\eta=\Phi_s-\Phi_m-V_{oc}$ on the cathode side,
Electric phase potential equation	$\nabla\cdot(\sigma_s\nabla\Phi_s)=-S_j$	$V_{oc}=1.23-0.9\times10^{-3}(T-298)+2.3\frac{RT}{4F}(\log p_{H_2}^2p_{O_2})$, $V_{cell}=V_{oc}-\eta_a-\eta_c-\eta_m$ $S_j=j_c$ on the cathode side, $S_j=-j_a$ on the anode side
Ionic phase potential equation	$\nabla\cdot(\sigma_m\nabla\Phi_m)=S_j$	$\sigma_m=\sigma_m^{ref}\exp\left[1268\left(\frac{1}{303}-\frac{1}{T}\right)\right]$, $\sigma_m^{ref}=0.005139\lambda-0.326$
Liquid water transport equation	$\nabla\cdot\left(\frac{\rho_lk_pk_{rl}}{\mu_l}\frac{\partial p_c}{\partial s}\nabla s\right)-\nabla\cdot\left(\frac{\rho_lk_pk_{rl}}{\mu_l}\nabla p_g\right)+\nabla\cdot\left(\frac{n_dM_{H_2O}}{F}\vec{i}_m\right)=S_L$	$n_d=2.5s$, $k_{rl}=s^3$, $k_{rg}=(1-s)^3$, $p_c=p_g-p_l$, $p_c=\sigma\cos\theta_c\left(\frac{\varepsilon}{k_p}\right)^{1/2}J(s)$, $J(s)=1.417(1-s)-2.120(1-s)^2+1.262(1-s)^3$, $\theta_c<90^\circ$, $J(s)=1.417s-2.120s^2+1.262s^3$, $\theta_c<90^\circ$
Water content in the membrane	$\nabla\cdot\left(\left(\frac{\alpha_dM_{H_2O}}{F}\vec{i}_m\right)\lambda-\left(\frac{M_{H_2O}\rho_{dry}}{M_m}D_\lambda\right)\nabla\lambda\right)=0$	$D_\lambda=D_\lambda^{ref}\exp\left(2416\left(\frac{1}{303}-\frac{1}{T}\right)\right)$, $D_\lambda^{ref}=10^{-10}\frac{\lambda}{(1+0.0126\lambda)a(17.81-79.7a+108a^2)D_\lambda'}$, $D_\lambda'=\begin{cases}\lambda/4 & \lambda\le2\\ 0.5+3.25(\lambda-2)/4 & \lambda\le6\\ 3.75+4(\lambda-26)/15 & \lambda>6\end{cases}$
Energy equation	$\nabla\cdot(\varepsilon(1-s)\rho_g\vec{u}_gC_{p,g}T)+\nabla\cdot(\varepsilon s\rho_l\vec{u}_lC_{p,l}T)$ $=\nabla\cdot(\lambda_{eff}\nabla T)+j\eta+\frac{i^2}{\sigma}+h_{fg}S_L$	$\lambda_{eff}=-2\lambda_s+\frac{1}{\frac{\varepsilon}{2\lambda_s+\lambda_f}+\frac{1-\varepsilon}{3\lambda_s}}$

Table 3 – Parameters of porous layers for sensitivity analysis.

Parameter	Porous layer	Benchmark value	Value	Unit
τ	Cathode GDL	1.5	1.0, 1.5, 2.0, 2.5, 3.0	–
	Cathode CL	1.5	1.0, 1.5, 2.0, 2.5, 3.0	–
	Anode GDL	1.5	1.0, 1.5, 2.0, 2.5, 3.0	–
	Anode CL	1.5	1.0, 1.5, 2.0, 2.5, 3.0	–
ε	Cathode GDL	0.5	0.3, 0.4, 0.5, 0.6, 0.7	–
	Cathode CL	0.4	0.3, 0.4, 0.5, 0.6, 0.7	–
	Anode GDL	0.5	0.3, 0.4, 0.5, 0.6, 0.7	–
	Anode CL	0.4	0.3, 0.4, 0.5, 0.6, 0.7	–
μ_p	Cathode GDL	1.76×10^{-10}	1.76×10^{-8}, 1.76×10^{-9}, 1.76×10^{-10}, 1.76×10^{-11}, 1.76×10^{-12}	m^2
	Cathode CL	1.76×10^{-11}	1.76×10^{-8}, 1.76×10^{-9}, 1.76×10^{-10}, 1.76×10^{-11}, 1.76×10^{-12},	m^2
	Anode GDL	1.76×10^{-10}	1.76×10^{-8}, 1.76×10^{-9}, 1.76×10^{-10}, 1.76×10^{-11}, 1.76×10^{-12},	m^2
	Anode CL	1.76×10^{-11}	1.76×10^{-8}, 1.76×10^{-9}, 1.76×10^{-10}, 1.76×10^{-11}, 1.76×10^{-12},	m^2
σ_s	Cathode GDL	500	1, 10, 53, 500, 1×10^4, 1×10^6	$\Omega^{-1}\,m^{-1}$
	Cathode CL	500	1, 10, 53, 500, 1×10^4, 1×10^6	$\Omega^{-1}\,m^{-1}$
	Anode GDL	500	1, 10, 53, 500, 1×10^4, 1×10^6	$\Omega^{-1}\,m^{-1}$
	Anode CL	500	1, 10, 53, 500, 1×10^4, 1×10^6	$\Omega^{-1}\,m^{-1}$
σ_m	Cathode CL	4.0	0.1, 0.5, 4.0, 20, 50, 100	$\Omega^{-1}\,m^{-1}$
	Anode CL	4.0	0.1, 0.5, 4.0, 20, 50, 100	$\Omega^{-1}\,m^{-1}$
λ	Cathode GDL	50	0.5, 5, 10, 50, 150	$W\,m^{-1}\,K^{-1}$
	Cathode CL	50	0.5, 5, 10, 50, 150	$W\,m^{-1}\,K^{-1}$
	Anode GDL	50	0.5, 5, 10, 50, 150	$W\,m^{-1}\,K^{-1}$
	Anode CL	50	0.5, 5, 10, 50, 150	$W\,m^{-1}\,K^{-1}$
	Membrane	10	0.5, 5, 10, 50, 150	$W\,m^{-1}\,K^{-1}$

The boundary conditions at the anode and cathode flow channels are that the inlet flow rates are constant, the inlet gas compositions are constant, and the flows are fully developed at the anode and cathode flow channel outlets. The solid walls are no slip with zero flux boundary conditions. At the interfaces between the gas channels, the GDLs, the catalyst layers, and the PEM, the velocities, mass fractions, momentum fluxes, and mass fluxes are assumed to be continuous. In the present model, the water in the membrane is assumed to be in vapor phase, thus, water content in the membrane and water vapor mass fraction in the catalyst layer should be equal at the interface between the membrane and the catalyst layer. Hence the following relation is used as boundary condition for the interface between the membrane and the catalyst layer to solve species equation of water vapor and water content equation in the membrane [1]:

$$\lambda = \begin{cases} 0.043 + 17.18a - 39.85a^2 + 36.0a^3 & 0 < a \le 1 \\ 14 + 1.4(a-1) & 0 < a \le 3 \\ 16.8 & a > 3 \end{cases} \quad (1)$$

The SIMPLE (Semi Implicit Method for Pressure-Linked Equation) algorithm was employed to solve the governing equations. The coupled set of equations was solved iteratively, with the solution considered to be converged when the relative error in each field between two consecutive iterations was less than 10^{-6}. The model used non-uniformly distributed elements in the x, y and z directions. The grid independence was examined in preliminary test runs.

3. Parameters for sensitivity analysis

Twenty nine parameters for sensitivity analysis are classified into two kinds. One is the structural or transport parameter of porous layers, including tortuosity, porosity, permeability, proton conductivity, electron conductivity, and thermal conductivity; the other is the electrochemical parameter, including anodic and cathodic exchange current densities, anodic and cathodic transfer coefficients for anode and cathode reactions. During individual parameter investigation, characteristic values for each parameter are chosen to analyze the effect of this parameter on the cell polarization curve with the other parameters equal to benchmark value (Tables 3 and 4). The polarization performance with benchmark parameters has been validated in our previous investigation [14].

Table 4 – Parameters for electrochemical reaction.

Parameter	Benchmark value	Value	Unit
$Aj_{0,a}^{ref}$	9.227×10^8	9.227×10^6, 9.227×10^7, 9.227×10^8, 9.227×10^9, 9.227×10^{10}	$A\,m^{-3}$
$Aj_{0,a}^{ref}$	1.05×10^6	1.05×10^3, 1.05×10^4, 1.05×10^5, 1.05×10^6, 1.05×10^7	$A\,m^{-3}$
$\alpha_{a,a}$	0.5	0.1, 0.3, 0.5, 0.7, 0.9	–
$\alpha_{a,c}$	0.5	0.1, 0.3, 0.5, 0.7, 0.9	–
$\alpha_{c,a}$	1.5	0.5, 1.0, 1.5, 2.0, 2.5	–
$\alpha_{c,c}$	1.5	0.5, 1.0, 1.5, 2.0, 2.5	–

The operation conditions are assumed to be as follows: cathode reactant is the humidified air with 100% relative humidity, 1.5 m s^{-1} inlet velocity and 323 K inlet temperature, and anode reactant is the humidified hydrogen with 100% relative humidity, 0.5 m s^{-1} inlet velocity and 323 K inlet temperature, the outlet pressure is set to be 1 atm. On the surface of bipolar plates, the isothermal boundary condition (323 K) is assumed for all parameter analyses.

4. Analysis

4.1. Tortuosity

Tortuosity τ of a porous medium is defined as the ratio of mean flow path of pore to thickness of the porous medium, thus $\tau \geq 1$. The lower limit of $\tau = 1$ means that the porous media is composed of multi-parallel capillary tubes. According to the relation $D_{eff} = D\varepsilon$ (1-s)$^{\tau}$, the effective diffusivity of gaseous species is dependent exponentially on tortuosity, especially at high liquid water saturation the effective diffusivity reduces significantly with tortuosity. The tortuosity is assumed to be 1.5 in a majority of the fuel cell models, which is derived from experimental test for porous sandy soil. However, the porous structure of GDLs and CLs is different from sandy soil. Hence, the tortuosity is set to 1.0, 1,5, 2.0, 2,5 and 3.0 to analyze its effect on the reactant transport and cell polarization curve.

Fig. 2 shows that as the tortuosity of cathode GDL and CL increases, the limiting current density and corresponding cell performance reduce remarkably, while the tortuosity of anode GDL and CL does not almost influence the cell performance. The effect of the tortuosity of cathode GDL and CL occurs at ohmic polarization regime ($V_{cell} < 0.7$ V) and becomes stronger at concentration polarization regime, which can be explained by liquid water saturation distribution in the cell. At high voltages, the electrochemical reaction rate is slow and only a limited amount of oxygen is consumed with only a small amount of liquid water produced, therefore, tortuosity has a small effect on the effective diffusivity of gaseous species. However, as the voltage is reduced, the reaction rate is increased and more liquid water is produced at cathode, the tortuosity becomes a dominant factor to the effective diffusivity. At the same liquid water saturation, increase in tortuosity reduces significantly the effective diffusivity and hence the cell performance. In addition, with the same tortuosity, higher liquid water saturation causes lower effective diffusivity, therefore, the effect of tortuosity is stronger at concentration polarization regime. The liquid water saturation at anode is far less than at cathode hence the tortuosity has a small effect on the effective diffusivity and cell performance.

The above analysis is proved in Figs. 3 and 4. Fig. 3 shows the liquid water saturations on the interface between the cathode GDL and CL for various tortuosities at $V_{cell} = 0.3$ V. The liquid water saturation under the rib is lower than that under the channel. The lowest saturation occurs at channel inlet, and the saturation is gradually increased along flow direction with the highest saturation at outlet under the rib. Larger tortuosity reduces liquid water removal and causes more

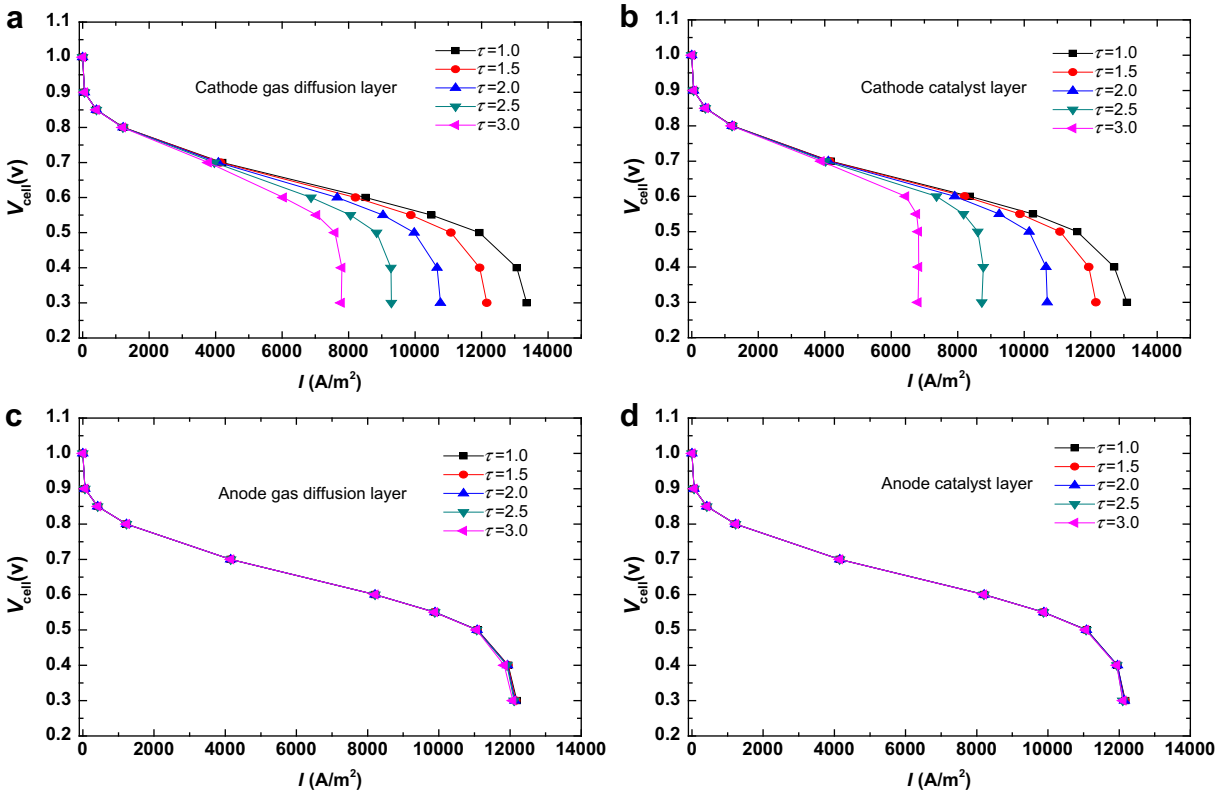

Fig. 2 – Polarization curves for various tortuosities of porous layers: (a) cathode GDL; (b) cathode CL; (c) anode GDL; (d) anode CL.

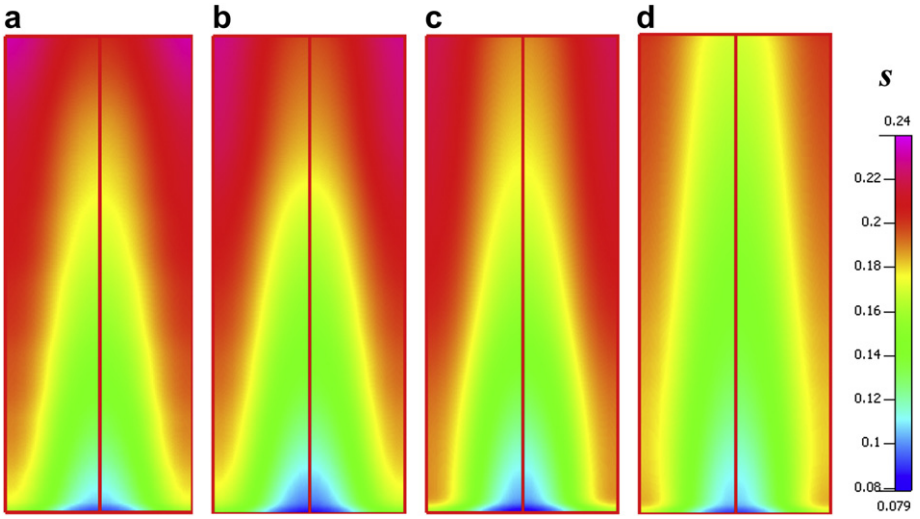

Fig. 3 – Liquid water saturations on the GDL-CL interface for various tortuosities of cathode CL at V_{cell} = 0.3 V: (a) τ = 1.5; (b) τ = 2.0; (c) τ = 2.5; (d) τ = 3.0.

liquid water accumulation in the porous GDL and CL, which decreases the effective diffusivity of oxygen and results lower local current density as shown in Fig. 4.

4.2. *Porosity*

Porosity ε is defined as the ratio of pore volume to total volume of a porous medium. Because high electron conductivity of 500 Ω^{-1} m^{-1} is adopted as benchmark value, the ohmic resistance of porous GDL and CL can be safely ignored, the porosity mainly influences the reactant transport and liquid water removal. The effect of porosity of porous layers on the cell polarization curve is shown in Fig. 5. It can be seen that the cathode GDL porosity has the strongest effect on the cell performance, following the cathode CL porosity, while the anode GDL and CL porosities have negligible effect. For example, as the cathode GDL porosity increases from 0.3 to 0.7, the current density rises by 36.1%, while for cathode CL the increment is only by 20.1%. The negligible effect of anode GDL and CL porosities can be explained by two reasons. First, liquid water saturation at anode is far less than that at cathode, so hydrogen transported to the anode catalyst layer can satisfy the need of electrochemical reaction even though at lower anode GDL and CL porosity. Second, hydrogen oxidation reaction is facile and hence the surface overpotential is small, the same transfer current density can be produced at lower hydrogen concentration. Oppositely, with large overpotential and high liquid water saturation, low cathode GDL and CL porosities reduce the oxygen transport to the cathode catalyst layer and reduce the electrochemical reaction rates, thus cell performance is declined.

4.3. *Permeability*

Permeability k_p represents the ability of fluid to flow through a porous media. Fig. 6 shows the effect of the porous GDL and CL permeabilities on the cell polarization curve. It is seen that as cathode GDL permeability is raised, the cell performance is

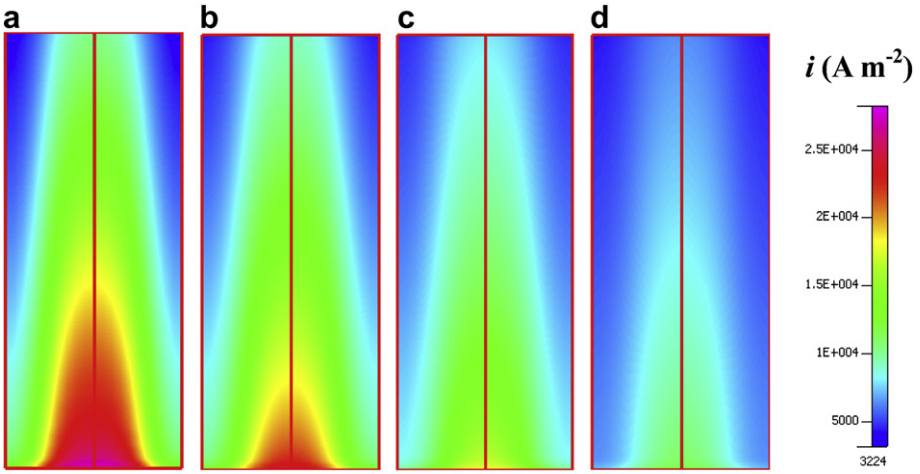

Fig. 4 – Current densities in the membrane for various tortuosites of cathode CL at V_{cell} = 0.3 V: (a) τ = 1.5; (b) τ = 2.0; (c) τ = 2.5; (d) τ = 3.0.

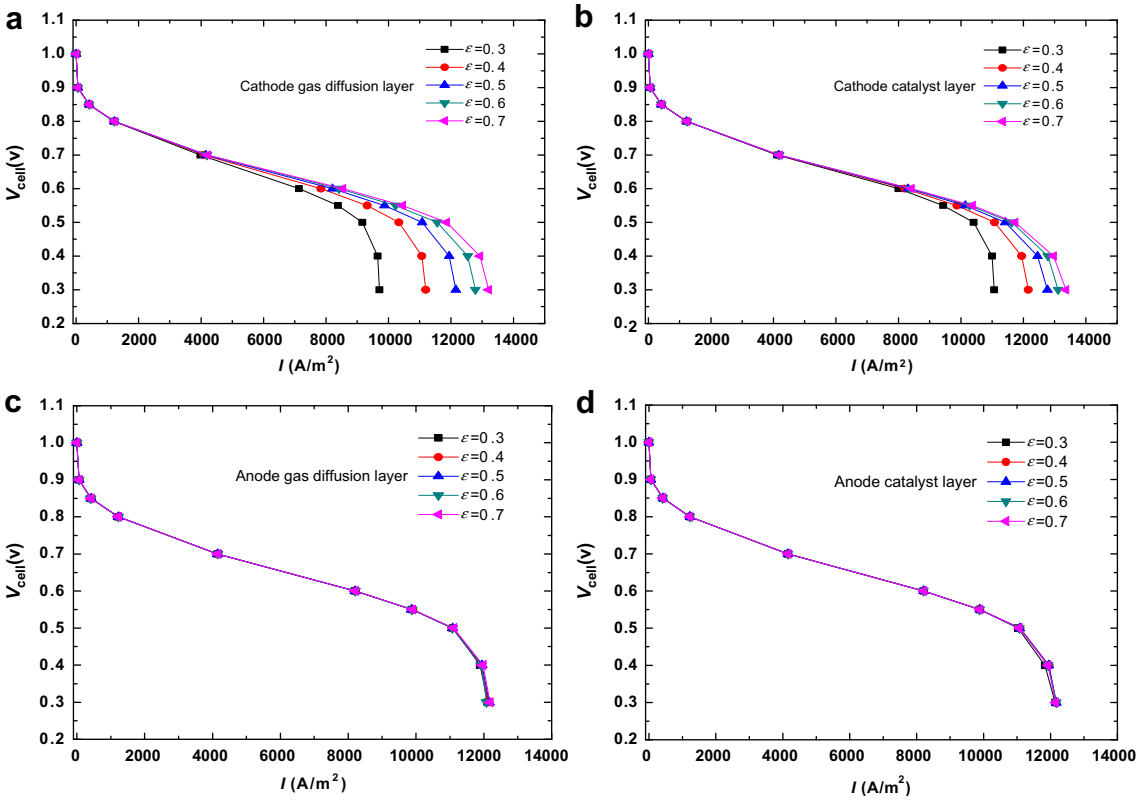

Fig. 5 – Polarization curves for various porosities of porous layers: (a) cathode GDL; (b) cathode CL; (c) anode GDL; (d) anode CL.

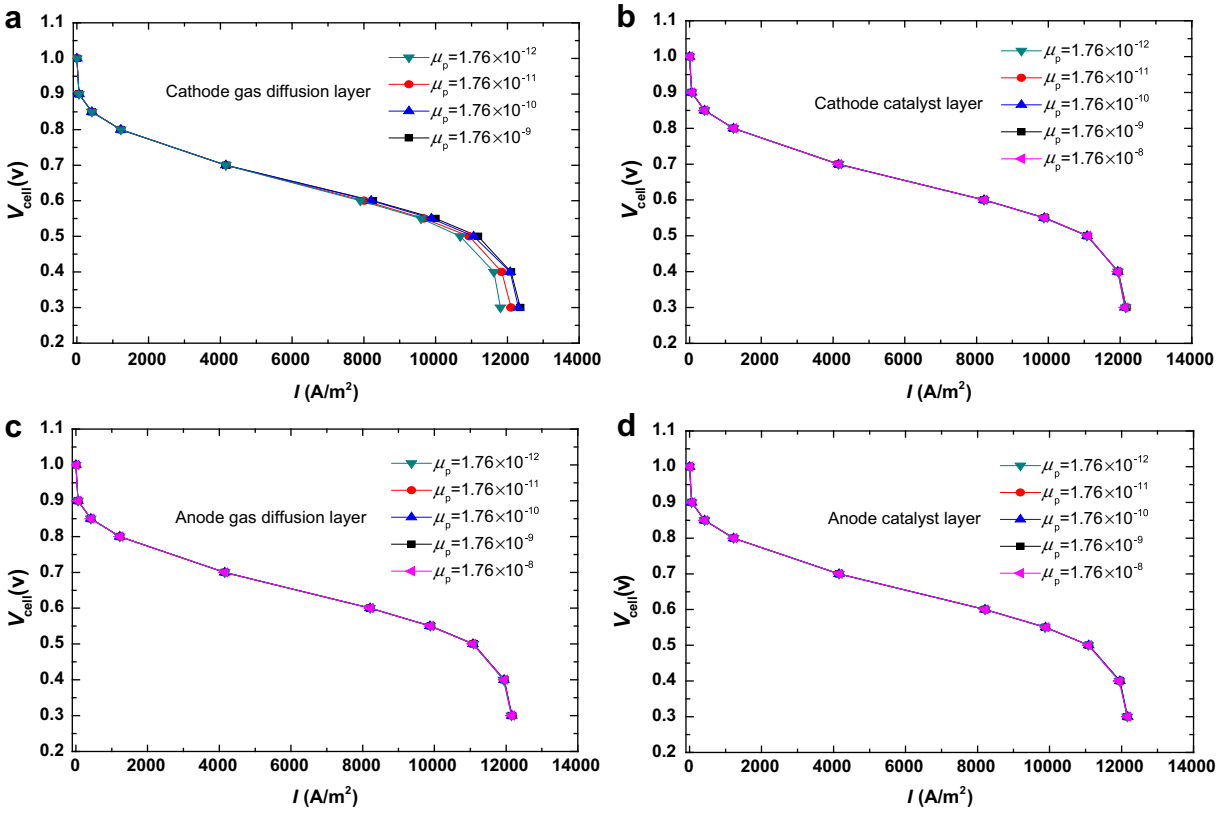

Fig. 6 – Polarization curves for various permeabilities of porous layers: (a) cathode GDL; (b) cathode CL; (c) anode GDL; (d) anode CL.

slightly increases at $V_{cell} < 0.6$ V, while the permeabilities of the other porous layers almost do not influence the cell performance. The limiting value of the cathode GDL permeability is 1.76×10^{-10}, greater than the value the increase in the cathode GDL permeability no longer increases the cell performance. The present analysis confirms that diffusion is dominant mechanism for reactant transport in the parallel flow field, but not pressure-driven transport, hence the permeability has a very small effect.

4.4. *Electron conductivity*

Polarization curves for various electron conductivities of porous layers are shown in Fig. 7. Because electrons produced by anode electrochemical reaction must be transported out of the cell and then be transported back to the anode catalyst layer, higher electron conductivity improves the cell performance. Fig. 7 shows that the GDL electron conductivity has far stronger effect on the cell performance than the CL electron conductivity. For low GDL electron conductivities of 1 and 10 Ω^{-1} m^{-1}, even though the operation voltage is reduced to 0.3 V, the cell is still in ohmic polarization regime and concentration polarization does not occur. The corresponding current densities are 209.9 and 6539.9 A m^{-2} for cathode GDL electron conductivities of 1 and 10 Ω^{-1} m^{-1}, and are 1089.9 and 6540.8 A m^{-2} for anode GDL electron conductivities of 1 and 10 Ω^{-1} m^{-1}, respectively. As the GDL electron conductivity is raised to 50 Ω^{-1} m^{-1}, concentration polarization occurs at low operation voltage, and the slope of ohmic polarization regime is increased significantly which means the improved cell performance. The limiting GDL electron conductivity is 500 Ω^{-1} m^{-1}, above which the increase in the GDL electron conductivity no longer improves the cell performance and concentration polarization becomes a dominant factor to determine the cell performance. The CL thickness (5 μm) is far less than GDL thickness (300 μm), due to low resistance of electron transport the cell performance is improved only a bit with increase in the CL electron conductivity.

4.5. *Proton conductivity*

Due to lack of appropriate model, in the previous models the CL proton conductivity is generally assumed to be constant or calculated by Springer model which is only applicable to the membrane. The constant proton conductivity is adopted in the present model in order to implement individual parameter analysis. Fig. 8 shows that the effect of the CL proton conductivity on the cell performance is far higher than that of the CL electron conductivity. Increase in the proton conductivity elevates the slope of ohmic polarization regime and hence improves the cell. With the proton conductivity higher than 4.0 Ω^{-1} m^{-1}, the CL has sufficient capacity to the conduction of protons produced by the electrochemical reaction, thus, the cell performance is no longer dependent on the CL proton conductivity. Further calculations indicate that the limiting proton conductivity is closely related to operation conditions. As the flow rate of reactants is raised, the amount of proton produced by electrochemical reaction is increased which causes an increased limiting proton conductivity.

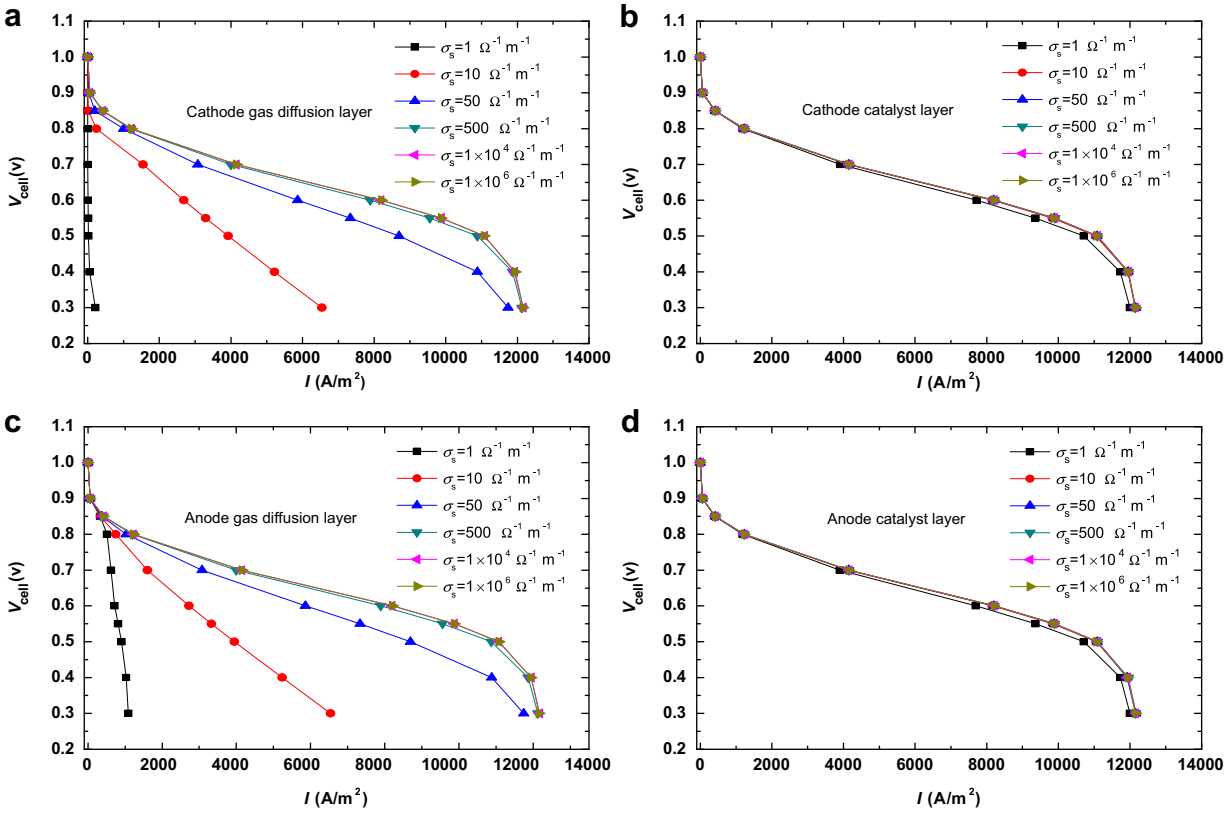

Fig. 7 – Polarization curves for various electron conductivies of porous layers: (a) cathode GDL; (b) cathode CL; (c) anode GDL; (d) anode CL.

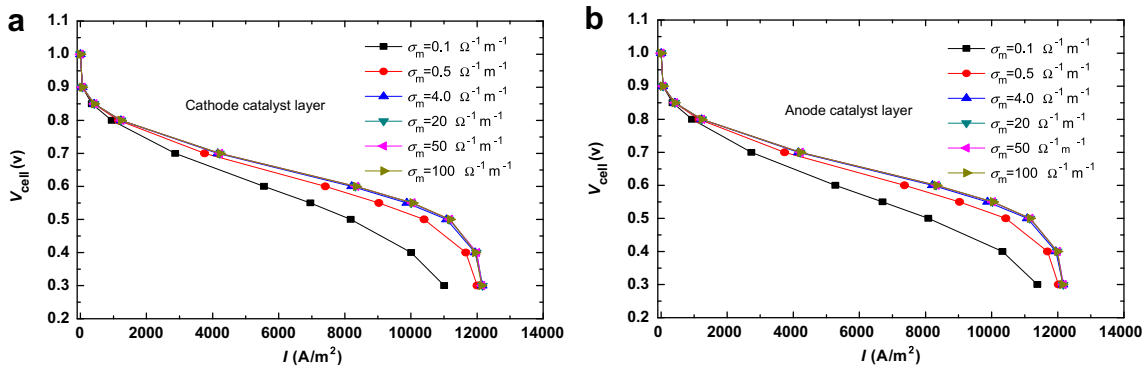

Fig. 8 – Polarization curves for various electron conductivies of catalyst layers: (a) cathode CL; (b) anode CL.

4.6. *Thermal conductivity*

The heat produced in the fuel cell mainly includes reaction heat, latent heat of phase change of water, and Joule heat. With high heat production rate and low heat removal capacity, the cell temperature will be elevated significantly, which causes worse membrane hydration and high proton transport resistance, thus, the cell performance is reduced. This argument has been confirmed by our previous investigation [15], where the convective thermal boundary condition was applied on surfaces of bipolar plates. With lower convective heat coefficient, the thermal conductivities of porous layers, especially thermal conductivities of GDLs, have remarkable effect on the cell performance. As the convective heat coefficient is increased, effect of thermal conductivity weakens. The isothermal thermal boundary condition is adopted and the temperature on the surfaces of bipolar plates is assumed to be 323 K equal to reactant inlet temperature in the present analysis, which causes a small temperature difference inside the cell, therefore, the same polarization curves are predicted with various thermal conductivities of porous layers (Fig. 9). It is noted that only polarization curves with various cathode GDL thermal conductivities are plotted in Fig. 9 because all curves coincide for the various thermal conductivities of anode GDL, cathode and anode CLs, and membrane. The present analysis indicates that with a good cooling effect, materials with a little lower thermal conductivity can also be used as porous electrode of fuel cell.

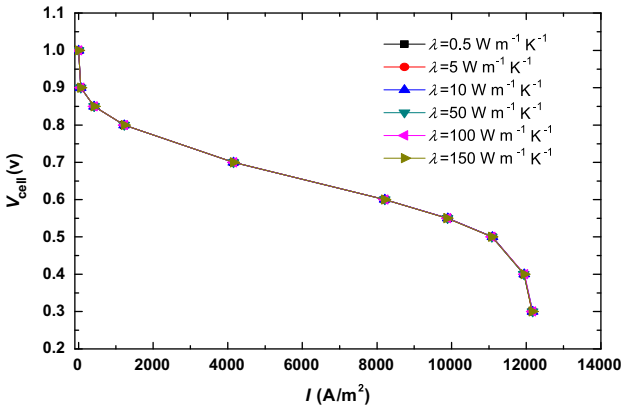

Fig. 9 – Polarization curves for various thermal conductivities of cathode GDL.

4.7. *Electrochemical reaction*

The electrochemical parameters include exchange current densities, and transfer coefficients at the cathode and anode. The cathode exchange current density is selected from 1.05×10^3 to 1.05×10^7 A m^{-3} with the anode exchange current densities ranging from 9.227×10^6 to 9.227×10^{10} A m^{-3} in the present analysis, which covers a wide range of values used in the previous models. The polarization curves for various exchange current densities are shown in Fig. 10. It can be seen that with the same operation condition, increase in the exchange current densities at the cathode and anode improves the cell performance due to higher transfer current densities produced by electrochemical reactions. The exchange current density influences significantly the activation potential. As the exchange current density is increased, the operation voltage at which activation polarization regime is converted into ohmic polarization regime is elevated; however, the slope of ohmic polarization remains almost unchanged. Larger exchange current density also means that more reactants should be provided for electrochemical reactions and hence concentration polarization occurs at higher operation voltage due to mass transfer limitations (Fig. 10). In addition, Fig. 10 also demonstrates that besides the case with $Aj_{0,a}^{ref} = 9.227 \times 10^6$A m^{-3}, there is a small difference in the limiting current densities for various exchange current densities because the limit of mass transfer is reached.

The general expressions of the Butler–Volmer equation are adopted in the present model, which includes four transfer coefficients: anodic and cathodic transfer coefficients for anode reaction, $\alpha_{a,a}$ and $\alpha_{a,c}$, and anodic transfer coefficient for cathode reaction, $\alpha_{c,a}$ and $\alpha_{c,c}$. Fig. 11 shows that $\alpha_{a,c}$ and $\alpha_{c,a}$ have a negligible effect on the cell performance, while $\alpha_{a,a}$ and $\alpha_{c,c}$ have remarkable effect. This can be explained by following reasons. The anode overpotential, η_a, is positive, the anode transfer current density is determined mainly by $\exp[\eta_a(\alpha_{a,a}F/(RT))]$ with a very small effect of $\exp[-\eta_a(\alpha_{a,c}F/(RT))]$ according to Butler–Volmer equation. Oppositely, cathode overpotential, η_c, is negative, the cathode transfer current density is determined mainly by $\exp[-\eta_c(\alpha_{c,c}F/(RT))]$. With the same current density, higher $\alpha_{a,a}$ and $\alpha_{c,c}$ cause a reduced

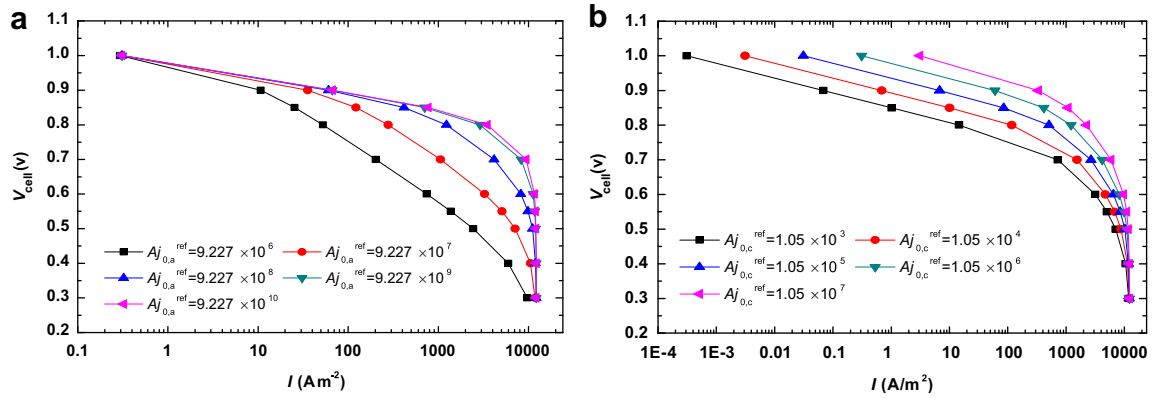

Fig. 10 – Polarization curves for various exchange current densities on cathode and anode (current density on log scale): (a) anode; (b) cathode.

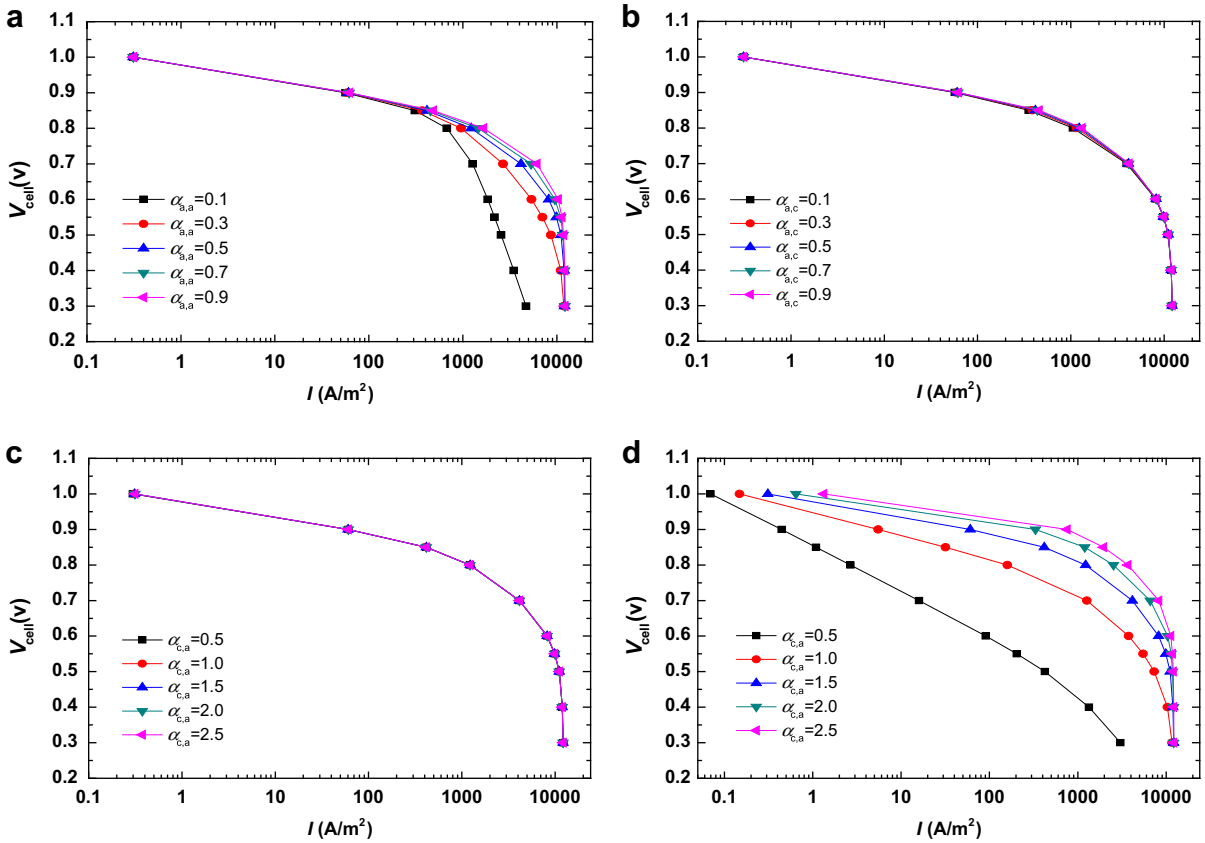

Fig. 11 – Polarization curves for various transfer coefficients (current density on log scale): (a) $\alpha_{a,a}$; (b) $\alpha_{a,c}$; (c) $\alpha_{c,a}$; (d) $\alpha_{c,c}$.

overpotential and increased operation voltage, thus, the cell performance is improved (Fig. 11). Fig. 10 also indicates that as $\alpha_{a,a}$ and $\alpha_{c,c}$ are increased, the current density at $V_{cell} = 0.3$ V is only slightly raised and there are the same limiting current densities for various $\alpha_{a,a}$ and $\alpha_{c,c}$.

5. Conclusions

A three-dimensional, two-phase, non-isothermal model is developed to implement the parameter sensitivity analysis for PEM fuel cell with parallel flow field design. Twenty nine key parameters are examined and divided into three groups, strongly sensitive, conditional sensitive and weak sensitive parameters according to its effect on the cell polarization curve. The results show that tortuosities and porosities of cathode GDL and CL, permeabilities of cathode GDL, electron conductivities of cathode and anode GDL, proton conductivities of cathode and anode CL, exchange current densities on cathode and anode sides, cathodic transfer coefficient on cathode side, and anodic transfer coefficient on anode side are strongly sensitive parameters, thermal conductivities of

porous layers are conditional sensitive parameters, and the others are weak sensitive. The optimization of parameters of cathode GDL and CL is more important to improve cell performance than that of anode GDL and CL because liquid water transport and removal significantly influence membrane hydration and reactant transport.

Acknowledgment

This study was supported by the National Natural Science Foundation of China (Nos. 51076009, 50825603, and U1034004), by National Basic Research Program of China (No. 2009CB219803), by Program for New Century Excellent Talents in University (No. NCET-11-0635), and by the Fundamental Research Funds for the Central Universities (No. 11ZG01).

REFERENCES

[1] Wang XD, Zhang XX, Yan WM, Lee DJ, Su A. Determination of the optimal active area for proton exchange membrane fuel cells with parallel, interdigitated or serpentine designs. Int J Hydrogen Energy 2009;34:3823–32.
[2] Chippar P, Kyeongmin O, Kang K, Ju H. A numerical investigation of the effects of GDL compression and intrusion in polymer electrolyte fuel cells (PEFCs). Int J Hydrogen Energy 2012;37:6326–38.
[3] Didierjean S, Lamibrac A, Geneston T, Rakotondrainibe A, Maranzana G, Rozier E, et al. Internal currents in response to a load change during fuel cell start-up. Int J Hydrogen Energy 2012;37:6798–807.
[4] Miao JM, Cheng SJ, Wu SJ. Metamodel based design optimization approach in promoting the performance of proton exchange membrane fuel cells. Int J Hydrogen Energy 2011;36:15283–9.
[5] Sohn YJ, Kim M, Yang TH, Kim K. Numerical analysis of convective and diffusive fuel transports in high-temperature proton-exchange membrane fuel cells. Int J Hydrogen Energy 2011;36:15273–82.
[6] Deevanhxay P, Sasabe T, Tsushima S, Hirai S. Investigation of water accumulation and discharge behaviors with variation of current density in PEMFC by high-resolution soft X-ray radiography. Int J Hydrogen Energy 2011;36:10901–7.
[7] Peighambardoust SJ, Rowshanzamir S, Hosseini MG, Yazdanpour M. Self-humidifying nanocomposite membranes based on sulfonated poly (ether ether ketone) and heteropolyacid supported Pt catalyst for fuel cells. Int J Hydrogen Energy 2011;36:10940–57.
[8] Kwon OJ, Kang MS, Ahn SH, Choi I, Lee KU, Jeong JH, et al. Development of flow field design of polymer electrolyte membrane fuel cell using in-situ impedance spectroscopy. Int J Hydrogen Energy 2011;36:9799–804.
[9] Boaventura M, Sousa JM, Mendes A. A dynamic model for high temperature polymer electrolyte membrane fuel cells. Int J Hydrogen Energy 2011;36:9842–54.
[10] Lu Z, Rath C, Zhang G, Kandlikar SK. Water management studies in PEM fuel cells, part IV: effects of channel surface wettability, geometry and orientation on the two-phase flow in parallel gas channels. Int J Hydrogen Energy 2011;36:9864–75.
[11] LaManna JM, Kandlikar SG. Determination of effective water vapor diffusion coefficient in PEMFC gas diffusion layers. Int J Hydrogen Energy 2011;36:5021–9.
[12] Wang XD, Duan YY, Yan WM, Peng XF. Local transport phenomena and cell performance of PEM fuel cells with various serpentine flow field designs. J Power Sources 2008;175:397–407.
[13] Huang YF, Kannan AM, Chang CS, Lin CW. Development of gas diffusion electrodes for low relative humidity proton exchange membrane fuel cells. Int J Hydrogen Energy 2011;36:2213–20.
[14] Wang XD, Huang YX, Cheng CH, Jang JY, Lee DJ, Yan WM, et al. An inverse geometry design problem for optimization of single serpentine flow field of PEM fuel cell. Int J Hydrogen Energy 2010;35:4247–57.
[15] Wang XD, Zhang XX, Yan WM, Lee DJ, Su A. Non-isothermal effects of single or double serpentine proton exchange membrane fuel cells. Electrochim Acta 2010;55:4926–34.
[16] Meng H. Multi-dimensional liquid water transport in the cathode of a PEM fuel cell with consideration of the micro-porous layer (MPL). Int J Hydrogen Energy 2009;34:5488–97.
[17] Suman B, Li J, Wang CY. Two-phase flow and maldistribution in gas channels of a polymer electrolyte fuel cell. J Power Sources 2009;187:431–43.
[18] Wang XD, Zhang XX, Liu T, Duan YY, Yan WM, Lee DJ. Channel geometry effect for proton exchange membrane fuel cell with serpentine flow field using a three-dimensional two-phase model. J Fuel Cell Sci Technol 2010;7:051019.
[19] Min CH. A novel three-dimensional, two-phase and non-isothermal numerical model for proton exchange membrane fuel cell. J Power Sources 2010;195:1880–7.
[20] Wang XD, Xu JL, Yan WM, Lee DJ, Su A. Transient response of PEM fuel cells with parallel and interdigitated flow field designs. Int J Heat Mass Trans 2011;54:2375–86.
[21] Akhtar N, Kerkhof PJAM. Effect of channel and rib width on transport phenomena within the cathode of a proton exchange membrane fuel cell. Int J Hydrogen Energy 2011;36:5536–49.
[22] Benziger J, Kimball E, Mejia-Ariza R, Kevrekidis I. Oxygen mass transport limitations at the cathode of polymer electrolyte membrane fuel cells. AIChE J 2011;57:2505–17.
[23] Qin CZ, Rensink D, Fell S, Hassanizadeh SM. Two-phase flow modeling for the cathode side of a polymer electrolyte fuel cell. J Power Sources 2012;197:136–44.
[24] Tao WQ, Min CH, Liu XL, He YL, Yin BH, Jiang W. Parameter sensitivity examination and discussion of PEM fuel cell simulation model validation Part I. Current status of modeling research and model development. J Power Sources 2006;160:359–73.
[25] Wang XD, Duan YY, Yan WM. Numerical study of cell performance and local transport phenomena in PEM fuel cells with various flow channel area ratios. J Power Sources 2007;172:265–77.
[26] Shimpalee S, Greenway S, Spuckler D, Van Zee JW. Predicting water and current distributions in a commercial-size PEMFC. J Power Sources 2004;135:79–87.
[27] Um S, Wang CY. Three-dimensional analysis of transport and electrochemical reactions in polymer electrolyte fuel cells. J Power Sources 2004;125:40–51.
[28] Hu M, Gu A, Wang M, Zhu X, Yu L. Three dimensional two phase flow mathematical model for PEM fuel cell: part I. Model development. Energy Convers Manage 2004;45:1861–82.
[29] Ye Q, Nguyen TV. Three-dimensional simulation of liquid water distribution in a PEM fuel cell with experimentally measured capillary functions. J Electrochem Soc 2007;154:B1242–51.
[30] Correa JM, Farret FA, Popov VA, Simoes MG. Sensitivity analysis of the modeling parameters used in simulation of proton exchange membrane fuel cells. IEEE Trans Energy Conversion 2005;20:211–8.